Research Square

Preprints are preliminary reports that have not undergone peer review.
They should not be considered conclusive, used to inform clinical practice,
or referenced by the media as validated information.

Mass transport and radial composition evolution during coagulation in dry-wet spinning of cellulose/TBAP/DMSO solutions

Yifan Jiao
Chinese Academy of Sciences
Ziwei Guo
Chinese Academy of Sciences
Hongliang Kang
Chinese Academy of Sciences
Ruigang Liu
rgliu@iccas.ac.cn

Chinese Academy of Sciences

Research Article

Keywords: Cellulose, TBAP/DMSO, Wet spinning, Coagulation, Diffusion kinetics

Posted Date: November 13th, 2026

DOI: https://doi.org/10.21203/rs.3.rs-11173923/v1

License: This work is licensed under a Creative Commons Attribution 4.0 International License.
Read Full License

Additional Declarations: No competing interests reported.

Mass transport and radial composition evolution during coagulation in dry-wet spinning of cellulose/TBAP/DMSO solutions

Yifan Jiao[a,b], Ziwei Guo[a,b], Hongliang Kang[a], Ruigang Liu[a,b,*]

[a] *Laboratory of Polymer Physics and Chemistry, Beijing National Laboratory of Molecular Sciences, Institute of Chemistry, Chinese Academy of Sciences, Beijing 100190, China.*

[b] *College of Chemistry, University of Chinese Academy of Sciences, Beijing 100049, China.*

Corresponding author, Email: rgliu@iccas.ac.cn.

Abstract

Component exchange and radial composition changes during coagulation were investigated for cellulose filaments spun from TBAP/DMSO solutions. Here, the exchange of water, dimethyl sulfoxide (DMSO), and tetrabutylammonium hydrogen phosphate (TBAP) in cellulose/TBAP/DMSO filaments was quantified by gravimetry and ^{1}H NMR. Fick's second law in cylindrical coordinates was used to estimate apparent diffusion coefficients and calculate radial composition paths. Experimentally determined pseudo-ternary cloud-point diagrams were then used to assess the onset of phase separation along these paths. Water exhibited the highest apparent diffusivity at low temperatures, while DMSO became the fastest at high temperatures and TBAP remained the slowest throughout. Increasing bath temperature shortened the period of net liquid uptake. At equal local water content, the maximum skin-core composition differences increased from 1.8 to 5.6 wt% for DMSO and from 2.3 to 5.8 wt% for TBAP as temperature increased from 10 to 70 °C. Adding DMSO to the bath generally reduced apparent diffusion and radial composition differences. Cellulose concentration had a limited effect on apparent diffusivity. This work links component transport to local composition changes during phase separation and provides a quantitative basis for selecting coagulation conditions to reduce radial composition heterogeneity.

Keywords

Cellulose, TBAP/DMSO, Wet spinning; Coagulation; Diffusion kinetics

Introduction

Cellulose is an abundant and renewable biopolymer (Schenzel et al. 2014) and has found wide applications in many fields (Kang et al. 2013, 2015; Klemm et al. 2005; Tu et al. 2021). Solution processing of cellulose includes the commercialized traditional viscose process (Quintana et al. 2024; Shen et al. 2023; Woodings 2001), Lyocell process based on *N*-methylmorpholine-*N*-oxide (Fink et al. 2001), and other emerging solvent systems, such as ionic liquids (ILs) (Swatloski et al. 2002; Zhang et al. 2005) and NaOH/urea aqueous system (Cai et al. 2008). In any solution process of cellulose, coagulation is one of the key steps for producing high-quality regenerated cellulose materials. Coagulation temperature and cellulose concentration can affect the morphology, pore size, and properties of regenerated cellulose films (Cai et al. 2007; Liu & Zhang 2009). In cellulose wet spinning, mass transport during coagulation, the exchange of solvent and coagulant between the coagulation bath and the solution filaments, governs the phase separation and the resulting filament formation. Quantitative transport data guide the selection of coagulation bath conditions and residence times for regeneration and washing. Coagulant uptake and solvent loss simultaneously shift the local filament composition toward the cloud-point boundary, where phase separation begins. Transport kinetics thus control both the composition pathway and the time required to reach this boundary. As cellulose solvent systems have evolved, each step increased the number of mobile components that must be individually quantified.

Early coagulation studies tracked the displacement of the coagulation boundary in NH_3/NH_4SCN and measured a solvent-nonsolvent mass-transport-rate difference (k) (Liu et al. 1989, 1990), which linked coagulation conditions to fiber cross-section and modulus without considering nonsolvent (water) uptake from solvent loss. In the coagulation steps of Lyocell process, direct measurements of water ingress and NMMO egress as distinct quantities were achieved (Biganska & Navard 2005), and the coagulation was further resolved into fast and slow apparent diffusion regimes in running filaments (Liu & Hu 2006). Later studies combined diffusion data with phase diagrams and SAXS/WAXS to link component fluxes to structural evolution (Ilyin et al. 2018; Nishiyama et al. 2019). Because NMMO-water contains only one solvent, these methods were not designed to track multiple solvent species simultaneously. Ionic liquids and quaternary ammonium salts subsequently expanded the set of solvents that directly dissolve cellulose. Their high viscosity, however, limits molecular diffusivity and causes resistance to flow during processing. Polar aprotic cosolvents such as dimethyl sulfoxide (DMSO) are therefore added as the cosolvent to reduce viscosity and increase diffusivity. For ILs, Hedlund et al. (2017) measured solvent egress and fitted the data to a Fick's second law model. The inclusion of DMSO, however, transforms coagulation from a binary exchange into a multi-component process, in which transport selectivity becomes an essential concept during coagulation. Research on quaternary ammonium salt/DMSO systems has focused on salt

dissociation and cellulose–solvent interactions (Idström et al. 2017; Wu, Zhong, et al. 2025).

Our previous work confirmed that the ditetrabutylammonium hydrogen phosphate/dimethyl sulfoxide (TBAP/DMSO) solvent system shows the excellent cellulose solubility, which is a promising system for the preparation of regenerated cellulose materials (Wu, Zhong, et al. 2025) and a new platform for further study of homogeneous cellulose reactions and functional cellulose materials (Wu, Guo, et al. 2025). For the purpose to use this solvent system to prepare regenerated cellulose fibers, the diffusion of the solvent and coagulant during the coagulation process of cellulose/TBAP/DMSO need to be investigate in detail. The previous investigation mainly focused on the mass transport, coagulation-front movement, or composition changes in planar samples during cellulose regeneration (Hedlund et al. 2017; Laity et al. 2002; Makarova et al. 2016; Zhang et al. 2019). The regeneration of cellulose from its TBAP/DMSO solutions is more complicated due to the usage of two-component solvent, which includes the diffusion of TBAP and DMSO out of the filaments and the diffusion of water into the filaments. The diffusion process of these components could influence the radial distributions of multiple components in a cellulose filament at the same stage of coagulation and hereafter influence the regeneration of cellulose.

Gravimetry and ^{1}H NMR were used together to track the time-dependent masses of water, DMSO, and TBAP in filaments during coagulation. A cylindrical form of Fick's second law was fitted to each component's data to yield apparent diffusion coefficients (Crank 1975; Jiang et al. 2011). Net mass gain was calculated as the cumulative difference between water uptake and the combined loss of DMSO and TBAP. Our results reveal that temperature does not accelerate all three components equally: the transport hierarchy changes with temperature, and the component dominates the cumulative mass balance shifts accordingly. Increasing DMSO concentration in the coagulation bath reduced all three apparent diffusion coefficients, whereas cellulose concentration in the solution has limited effect. Based on the measured apparent diffusion coefficients of different components, the radical distributions of multiple components in a cellulose filament were investigate in detail. Experimentally determined pseudo-ternary cloud-point diagrams provided a reference. These component-resolved data provide important information for optimizing coagulation parameters.

Materials and methods

Preparation of cellulose/TBAP/DMSO solution

Tetrabutylammonium hydroxide (TBAH, 40 wt% aqueous solution), phosphoric acid (≥85.0%), dimethyl sulfoxide (DMSO, 99.5%), and other reagents were purchased from commercial suppliers and used as received. Pyridine (99.9%) was purified by distillation before use. Cotton linter pulp (Shandong Yinying Co., Ltd., China) was dried under vacuum at 80 °C overnight before use. The degree of polymerization of cotton linter pulp is 800, as determined

by intrinsic viscosity method in copper ethylenediamine (CED) solution at 25 °C (Marx 1955).

TBA_2HPO_4 (TBAP) was prepared according to our previous work (Wu, Zhong, et al. 2025). Cellulose solutions containing 4, 6, 7, or 8 wt% cellulose were prepared in DMSO/TBAP with a fixed mass ratio of 1.5. Each mixture was stirred at 60°C for 15 min to obtain a homogeneous solution and then centrifuged at 10,000 rpm for 3 min to remove entrained air. The resulting spinning dopes were transferred to the spinning reservoir.

Conditions of dry-wet spinning and coagulation

Dry-wet spinning was performed using a home-made apparatus. The cellulose/TBAP/DMSO dope was extruded through a single-orifice spinneret with an internal diameter of 0.40 mm under a nitrogen pressure of 0.20 MPa. The air gap between the spinneret and the coagulation bath was fixed at 20 mm and the spinning speed was fixed at 0.2 m/s. Before spinning, the dope mass flow rate was determined by weighing the dope extruded over a fixed period. The effect of bath temperature was investigated using 7wt% cellulose solution and water bath at 10, 30, 50, and 70°C, and the effect of bath composition was examined at 25°C using 7wt% cellulose solution and aqueous bath containing 0, 10, 20, 30, or 40 wt% DMSO. The volume ratio of extruded dope to coagulation bath was maintained at approximately 1:400 in each experiment to minimize changes in the bulk bath composition.

Measurement of the composition in the running filament

The average mass of DMSO and TBAP in the running filaments were determined as follows: Filament samples were collected at different distances along the coagulation bath. The coagulation time was calculated from the traveled distances and the filament velocity. The coagulation bath liquid adhering to the filament surface was carefully removed using absorbent paper, and each filament was immediately weighed to obtain its wet mass, m_t. The filament was then immersed in a known mass of deionized water for 2 h to completely extract the remaining DMSO and TBAP. After solvent exchange, the filament was removed, blotted using the same procedure, and weighed to obtain its equilibrium wet mass after extraction in deionized water, m_{eq}. It was subsequently dried to constant mass to obtain the dry cellulose mass, m_{dry}. A known mass of the resulting aqueous extract was taken for ^{1}H NMR to obtain the mass of DMSO and TBAP. Three independent samples were analyzed at each coagulation time.

Purified pyridine was used as the internal standard for ^{1}H NMR. For each sample, known mass of the aqueous extract and the internal standard solution were mixed and transferred to an NMR tube. The ^{1}H NMR spectra were recorded on a Bruker AVANCE III HD 400 MHz NMR spectrometer at room temperature. The amounts of DMSO and TBA^+ were determined from the ratios of their peak integrals to the pyridine peak integral, with correction for the number of protons represented by each signal. The mass of TBAP was calculated from the TBA^+ amount using a 2:1 molar ratio of TBA^+ to TBAP.

Cloud-Point Titration Experiments

Cellulose/TBAP/DMSO solutions containing 0.1, 0.5, 1.0, 1.5, or 2.0 wt% cellulose were prepared. Deionized water was added stepwise in known volumes. After each addition, the sample was sonicated in a temperature-controlled ultrasonic bath to promote mixing and was then allowed to reach thermal equilibrium. Transmittance was subsequently measured using a UV-Vis spectrophotometer. Water addition continued until a marked decrease in transmittance persisted after sonication and thermal equilibration, and the corresponding composition was taken as the cloud point. Each titration was performed in triplicate.

Accordingly, the phase behavior of this pseudo-ternary system can be analyzed using the theoretical framework proposed by (Boom et al. 1993). The LCP equation is applicable to liquid-liquid demixing in both dilute and concentrated polymer solutions. Therefore, cloud-point compositions over the entire composition range were determined by fitting and extrapolation, enabling construction of the complete cloud-point binodal.

Theoretical calculations

Calculations of apparent diffusion coefficients

During the coagulation, the diffusion of the solvent and nonsolvent components can be described independently by Fick's second law,

$$\frac{\partial c}{\partial t} = D_{app}\left(\frac{\partial^2 c}{\partial r^2} + \frac{1}{r}\frac{\partial c}{\partial r}\right) \tag{1}$$

where c is the component concentration, t is the coagulation time, r is the radial coordinate, and D_{app} is the apparent diffusion coefficient. The filament was approximated as a cylinder with a constant radius (R). Axial diffusion was neglected.

For DMSO and TBAP diffusing out of the filament into coagulation bath, the remaining mass fraction was expressed as,

$$\frac{M_i(t)}{M_0} = 4\sum_{n=1}^{\infty}\frac{1}{\lambda_n^2} exp\left(-\frac{\lambda_n^2 D_{app} t}{R^2}\right) \tag{2}$$

For water diffusing into the filament, the normalized uptake was expressed as,

$$\frac{M_i(t)}{M_\infty} = 1 - 4\sum_{n=1}^{\infty}\frac{1}{\lambda_n^2} exp\left(-\frac{\lambda_n^2 D_{app} t}{R^2}\right) \tag{3}$$

where $M_i(t)$ is the mass of the TBAP, DMSO, and water in the filament at time t, m_0 is the initial mass of TBAP and DMSO in cellulose solution, m_∞ is the equilibrium water mass in the filaments, and λ_n is the nth positive root of $J_0(\lambda_n) = 0$. The experimental mass ratios were fitted by nonlinear least squares using Eqs. 2 and 3 using the measured data of R, m_0 and m_∞ to result D_{app}.

Coagulation is a mass transport process in which the local diffusion coefficients change continuously with composition. Therefore, a single constant D cannot directly describe the

initial mass transport rate. Previous studies have shown that the cumulative transferred mass of each component is approximately linear with $t^{1/2}$ over short time. Its slope can therefore be defined as the rate coefficient k_i to compare the initial mass transfer rates of different components expressed as,

$$\frac{\Delta M_i(t)}{\Delta M_{i,\mathrm{eq}}} = k_i\sqrt{t} \tag{4}$$

where $\Delta M_i(t)$ is the cumulative exchanged mass of component *i* at time *t*, and $\Delta M_{i,eq}$ is the final value of the cumulative exchanged mass at equilibrium. When the experimental data satisfy $\Delta M_i(t)/\Delta M_{i,eq} < 0.60$, the data points can be fitted by linear regression to result k_i from the slope of fitting line. Initial mass transport kinetics were first quantified using the component mass. The cumulative transferred mass was calculated as follows,

$$\Delta M_i(t) = M_i(t) - M_i(0) \tag{5}$$

Thus the cumulative transferred mass of the solvent system TBAP and DMSO, the nonsolvent (water) can be calculated by $\Delta M_{water}(t) = M_{water}(t) - M_{water}(0)$, and the cumulative transferred mass for DMSO and TBAP can be calculated by $\Delta M_i(t) = M_i(0) - M_i(t)$, where $M_i(t)$ is the remaining mass of component *i* in the filament at time *t*.

Net mass gain (NMG) represents the normalized net change in filament mass during coagulation and reflects the balance between water influx and the outflux of TBAP and DMSO, which is calculated by,

$$NMG(t) = \frac{m_{wet} - \alpha\Delta t_{\mathrm{collection}}}{\alpha\Delta t_{\mathrm{collection}}} \tag{6}$$

where m_{wet} is the wet filament mass, α is dope flow rate (g/min), and $\Delta t_{\mathrm{collection}}$ is the duration of sample collection in minutes.

Numerical calculation of radial composition evolution

The radial component distribution was calculated as follows. The model based on Fick's second law was established by using the experimentally determined D_{app} of water, DMSO, and TBAP. The filament was approximated as a cylinder with a fixed radius of R = 200 μm. The initial and boundary conditions were defined as follows: At the filament center, the radial mass flux was set to zero, and at the filament surface, the composition was fixed at the equilibrium value specified by the coagulation bath. The equilibrium compositions measured by gravimetry and ^{1}H NMR were approximately consistent with the boundary values used in the simulations. The filament radius was divided into nine equal intervals (**Figure 1**). Model results were recorded at ten radial positions of r/R = 0-0.9. The surface (r/R = 1.0) was used to impose the boundary condition and excluded from the plotted data. The model was evaluated in the range of 0-50 s at intervals of 0.5 s. The calculation was implemented in Python using NumPy and SciPy.

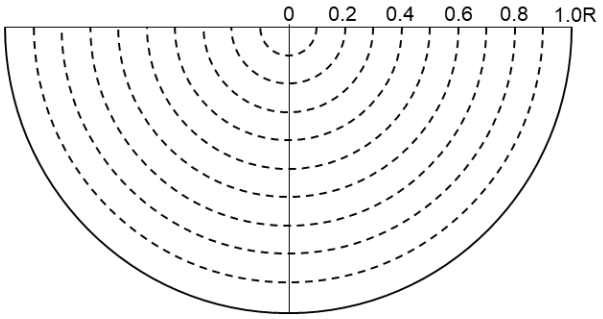


Fig. 1 Schematic illustration of the radial discretization of the filament cross-section. *R* is the filament radius, *r* is the radial distance from the center, and *r* = *R* represents the filament surface

For each coagulation condition, the model calculated $n_i(r,t)$, the fraction of local exchange completed for component i at position r and time t. It increases from 0 initially to 1 at equilibrium.

The normalized component mass, $q_i(r,t)$, was defined as the local mass of component *i* divided by the initial local total mass. It was calculated from the local exchange fraction, $n_i(r,t)$, as follows. For water entering the filament,

$$q_{water}(r,t) = n_{water}(r,t)q_{water,eq} \tag{7}$$

For DMSO and TBAP leaving the filament,

$$q_i(r,t) = q_{i,eq} + (1 - n_i(r,t))(q_{i,0} - q_{i,eq}) \tag{8}$$

where i represents DMSO or TBAP, and $q_{i,0}$ and $q_{i,eq}$ are the initial and equilibrium values, respectively. In case of coagulation in pure water, $q_{water} = 0.93n_{water}(r,t)$, $q_{DMSO} = 0.558(1 - n_{DMSO})$, $q_{TBAP} = 0.372(1 - n_{TBAP})$, and $q_{cellulose} = 0.07$.

The local mass fraction of component *i*, $w_i(r,t)$, was calculated by dividing $q_i(r,t)$ by the sum of the normalized masses of all components as follow,

$$w_i(r,t) = \frac{q_i(r,t)}{q_{water}(r,t) + q_{DMSO}(r,t) + q_{TBAP}(r,t) + q_{cellulose}(r,t)} \tag{9}$$

The calculation yielded the composition of each component at different radial positions and coagulation times.

The phase separation paths at different radial positions were compared at same coagulation bath temperature, clarifying the effect of mass transport on the radial phase separation path. Instead of coagulation time, $w_{water}(r,t)$ was used to represent coagulation progress, which is nonsolvent-induced phase separation (NIPS). $w_i(0.1R,t)$ and $w_i(0.9R,t)$ represent the core and skin region, respectively. Based on the model of water mass transport, the time at same w_{water} of $0.1R$ and $0.9R$ was determined. Then, the mass fractions of DMSO, TBAP, and cellulose were calculated. And $w_{water}(r,t)$ were set at intervals of 1.0 wt%, ranging from 0 to the corresponding equilibrium value.

Results and discussion

Net mass gain and diffusion coefficients

Fig. 2 shows the time dependence of net mass gain (NMG) at the denoted temperature of coagulation bath, following Eq. 6. At lower temperatures, NMG initially increased to a positive maximum and then decreased, eventually becoming negative. Positive NMG indicates that cumulative water uptake exceeded the combined loss of DMSO and TBAP. The subsequent decrease indicates a reduction in net mass gain, while the zero crossing marks the point at which cumulative water uptake equaled cumulative solvent loss. As the bath temperature increased, the maximum NMG decreased and the zero crossing marks occurred earlier. At 70 °C, NMG was negative from the first measured time point. These changes raise the question of how the three components respond differently to temperature.

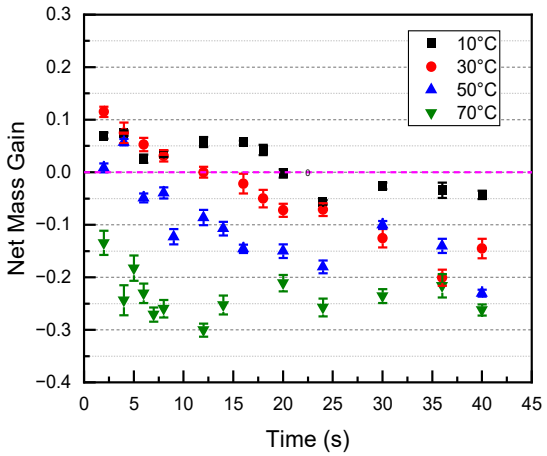


Fig. 2 Net mass gain of the filaments as a function of residence time at different temperature

To identify the component contributions to the change in NMG, the initial exchange kinetics were compared using the apparent mass transport rate coefficient k_{app}. **Fig.3** shows the typical plots of the normalized cumulative transferred mass $\Delta M_i(t)/\ \Delta M_{i,eq}(t)$ as a function of $t^{1/2}$ for water, DMSO, and TBAP at the initiating stage of the coagulation ($\Delta M_i(t)/\ \Delta M_{i,eq}(t) < 0.6$). The experimental data were fitted using Eq. 4 to result k_{app} (**Table 1**). The k_{app} values of all three components in the present work increase with increasing coagulation bath temperature, but their relative order changes (**Figure 4**). TBAP exhibits the lowest k_{app} at all temperatures. At 10 and 30 °C, the k_{app} of water is slightly higher than that of DMSO, whereas at 50 and 70 °C, the k_{app} of DMSO is higher than that of water. This change is consistent with the temperature dependence of NMG. At low temperature, nonsolvent uptake exceeds solvent loss during initial coagulation, resulting in net liquid uptake. With increasing temperature, the enhanced outward transport of DMSO allows the solvent loss to balance nonsolvent uptake at an earlier time.

The changes in k_{app} at different temperatures can be interpreted by considering the mobility of the medium and the characteristics of the diffusing molecule. First, at low temperature, the high viscosity of the cellulose solution restricts the transport of all components. With increasing

temperature, the mobility of the medium increases, which accelerates the transport of the diffusing species. This enhancement is stronger for the larger species, so that at higher temperatures the outward transport of DMSO eventually exceeds the inward transport of water. Secondly, there is a strong bonding of the TBAP molecules to the cellulose chain, which slows down the detachment of the TBAP molecules from the chain. This bonding keeps TBAP the slowest component over the whole investigated temperature range. Furthermore, the DMSO and TBAP are more bulky than the water molecule, which should also decrease their apparent transport rates. These characteristics can explain why the k_{app} at low temperatures follows the order of water, DMSO, and TBAP.

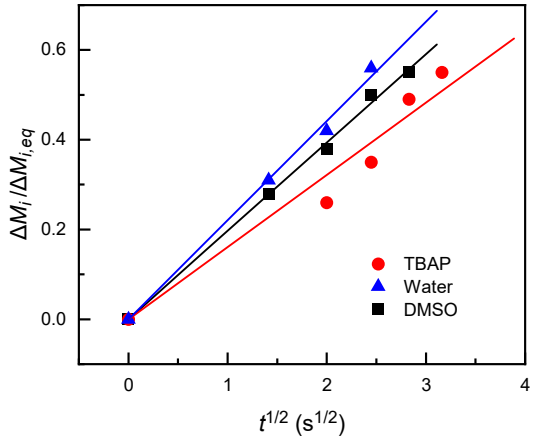


Fig. 3 Normalized cumulative transferred mass for each component in the solution at 30 °C, displaying the linearity to $t^{1/2}$ and the evaluation of the respective rates, for short times

Table 1 Summary of Rate Coefficients Obtained Using Eqs. 2-6

Temperature (°C)	$k_{app,water}$ ($s^{-1/2}$)	$k_{app,DMSO}$ ($s^{-1/2}$)	$k_{app,TBAP}$ ($s^{-1/2}$)
10	0.1825	0.1742	0.1485
30	0.2208	0.1968	0.1608
50	0.2264	0.2419	0.1831
70	0.2700	0.2857	0.2165

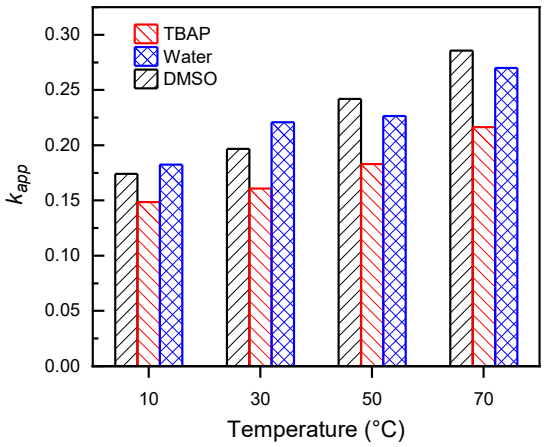


Fig. 4 The k_{app} for each chemical component at coagulation bath temperatures of 10, 30, 50, and 70 °C

Apparent diffusion coefficients

Fig. 4 shows the normalized mass profiles of DMSO, TBAP, and water in the filament as a function of the residence time in the coagulation bath at different temperatures. The lines are the fitting results according to Eq. 2 for TBAP and DMSO, and Eq. 3 for water, from which the apparent diffusion coefficients of all components were obtained and listed in **Table 2**. As expected, the higher the bath temperature, the faster the DMSO and TBAP release from the nascent fiber, and the faster cellulose regeneration. At 10 and 30 °C, $D_{app,water}$ was higher than $D_{app,DMSO}$ and $D_{app,TBAP}$. The D_{app} values of water and DMSO were similar at 50 °C, whereas DMSO had the higher value at 70 °C. The apparent diffusion coefficient was plotted as a function of $1/T$ and fitted by Arrhenius equation to obtain the activation energy for this system (**Figure 6**). The resulting activation energies are E_{DMSO} = 13.83 kJ/mol, E_{water} = 9.36 kJ/mol, and E_{TBAP} = 8.89 kJ/mol. The higher activation energy of DMSO indicates that its apparent diffusion is sensitive to temperature, which might relate to the specific interactions in the system. Our previous results confirmed that DMSO promotes the dissociation of TBAP into TBA^+ and HPO_4^{2-}. HPO_4^{2-} forms hydrogen bonds with cellulose hydroxyl groups and disrupts the original hydrogen-bond network, whereas DMSO solvates TBA^+ and facilitates its distribution around the cellulose chains (Wu, Zhong, et al. 2025). In contrast to TBAP, DMSO interacts only weakly with cellulose. Its mobility is therefore expected to depend more strongly on the viscosity than on direct association with cellulose.

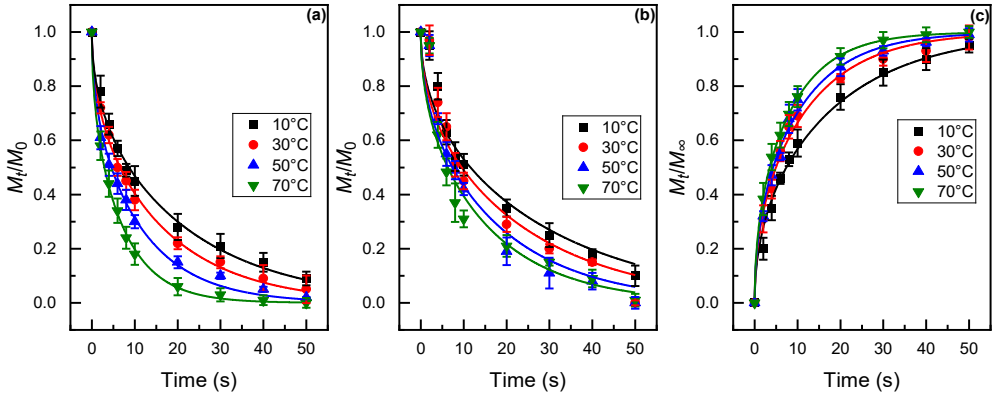


Fig. 5 Normalized mass profiles of (a) DMSO, (b) TBAP, and (c) water in the filaments during coagulation at different temperature. Water was used as the coagulant and the spinning dope with cellulose concentration of 7 wt%. Lines in (a) and (b) were the fitted results using Eq. 2 and lines in (c) were the fitted results using Eq. 3

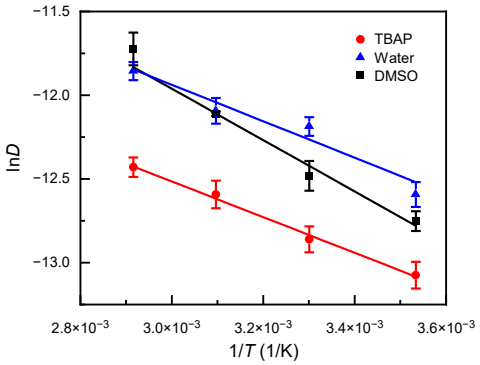


Fig. 6 Arrhenius plot for DMSO, TBAP, and water diffusion coefficients for 7 wt.% cellulose solutions

Fig. S1 shows the normalized mass profiles of the TBAP, DMSO, and water in the coagulation procedure at in the case of using cellulose/TBAP/DMSO solutions with different cellulose concentration, and the lines are the fitting results by using Eq. 2 for TBAP and DMSO, Eq. 3 for water to result the apparent diffusion coefficient (**Table 2**). The results indicate that D_{app} of all components only decrease slightly with increasing cellulose concentration, consistent with the Fricke obstruction model. The cellulose structures formed during coagulation may act as impermeable obstacles to increase the tortuosity of the diffusion paths and thus reduces the diffusion (Frickl 1924; Oh et al. 1996). Furthermore, interactions between cellulose and the solvent should also be considered. In a similar TBAAc/DMSO/cellulose system, Idström et al. (2017) found that the self-diffusion coefficients of TBA^+, acetate, and DMSO decreased with increasing cellulose concentration, with acetate showing the largest decrease. These decreases reached tens of percent relative to the solvent without cellulose and were larger than expected from excluded-volume effects alone. Although self-diffusion coefficients are not directly equivalent to D_{app}, the much weaker concentration dependence observed here suggests that mass transport during coagulation may be controlled less by molecular mobility in the initial homogeneous solution and more by the liquid-rich transport pathways formed during phase separation.

Fig. 7 shows normalized mass profiles of DMSO, TBAP, and water in the filaments during coagulation in the coagulating bath with different DMSO content at 25 °C. The lines are the fitting results using Eq. 2 for DMSO and TBAP, Eq. 3 for water and the obtained D_{app} are listed in Table 2. The results show that D_{app} values of all the components decrease with increasing DMSO content in the coagulation bath, from 0 to 40 wt %. Specifically, the $D_{app,water}$ decreases from 4.4 to 1.1×10^{-10} m^2/s, that of DMSO decreases from 3.8 to 0.8×10^{-10} m^2/s, and that of TBAP decreased from 2.2 to 0.7×10^{-10} m^2/s. Considering the influence of bath composition on diffusion, it is reasonable that the slower mass transport at higher DMSO contents is mainly due to the reduced concentration difference between the filament and the coagulation bath. This smaller difference lowers the driving force for the exchange and slows the overall mass transport process. Similar effects of bath composition have been reported for cellulose coagulation systems (Guizani et al. 2021). Moreover, a softened coagulation bath changes the morphology and compactness of the developing surface layer (Makarova et al. 2016), which can limit subsequent mass transfer (Holda & Vankelecom 2015).

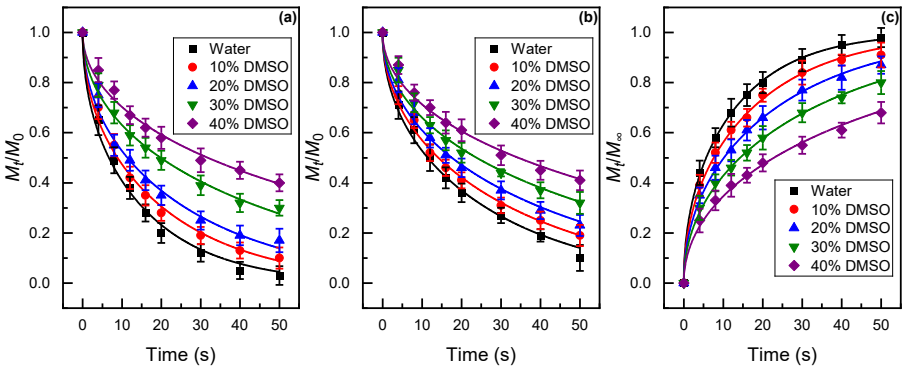


Fig.7 Normalized mass profiles of (a) DMSO, (b) TBAP, and (c) water in the filaments during the coagulation in the coagulation bath with different content of DMSO. Temperature of the coagulation bath was set at 25 °C. Cellulose concentration in the spinning dopes is 7 wt%. Lines in (a) and (b) were the fitted results using Eq. 2 and lines in (c) were the fitted results using Eq. 3

The D_{app} values of DMSO, TBAP, and water under all the investigated conditions are summarized in **Table 2**. The D_{app} values obtained here should be treated as apparent parameters for the given coagulation conditions and time ranges, rather than representing intrinsic diffusion coefficients. The D_{app} values depend strongly on temperature and coagulation bath composition, but only weakly by cellulose concentration within the investigated range. The D_{app} values in this study range from 0.7 to 8.1×10^{-10} m^2/s, in the same order of magnitude as those reported for other cellulose coagulation systems, approximately 0.4 to 8.0×10^{-10} m^2/s for cellulose/NMMO systems (Biganska & Navard 2005; Liu & Hu 2006), 0.23 to 1.55×10^{-10} m^2/s for IL systems (Hauru et al. 2016), and 2.10 to 4.33 $\times10^{-10}$ m^2/s for the [C2mim][OAc]/DMSO/cellulose water system (Hedlund et al. 2017). However, quantitative comparisons across studies require caution because the estimated coefficients depend on the experimental approach and diffusion models employed.

Table 2 The D_{app} of water, DMSO, and TBAP at different cellulose concentrations or coagulation bath conditions

Cellulose conc. (wt%)	Bath temperature (°C)	DMSO in bath (wt%)	Diffusion coefficient ($\times10^{-10}m^2/s$)		
			DMSO	TBAP	Water
7	10	0	2.9	2.1	3.4
	30		3.8	2.6	5.1
	50		5.5	3.4	5.6
	70		8.1	4.0	7.1
7	25	0	3.8	2.2	4.4
		10	2.8	1.8	3.4
		20	2.2	1.4	2.5
		30	1.3	1.1	1.7
		40	0.8	0.7	1.1
4	25	0	4.9	3.3	5.4
6			4.2	2.7	5.1
7			3.8	2.3	4.3
8			3.6	2.2	4.1

Radial composition distribution and phase separation path

The preceding analysis quantified the overall exchange of water, DMSO, and TBAP but did not resolve their local compositions across the filament. The experimentally determined D_{app} values were therefore used to calculate radial composition evolution using Eqs. 7-9 and the radial discretization shown in **Fig. 1**. **Fig. 8** shows the calculated local mass fractions of DMSO, TBAP, and water as functions of coagulation time at different radial positions and bath temperatures. The near-surface region changed first: the water fraction increased, while the DMSO and TBAP fractions decreased. Changes near the core occurred later, and increasing bath temperature accelerated component exchange. However, these time-dependent profiles do not clearly distinguish the composition paths at different radial positions. The local compositions at $0.1R$ and $0.9R$ were therefore compared at the same local water mass fraction, $w_{water}(r,t)$.

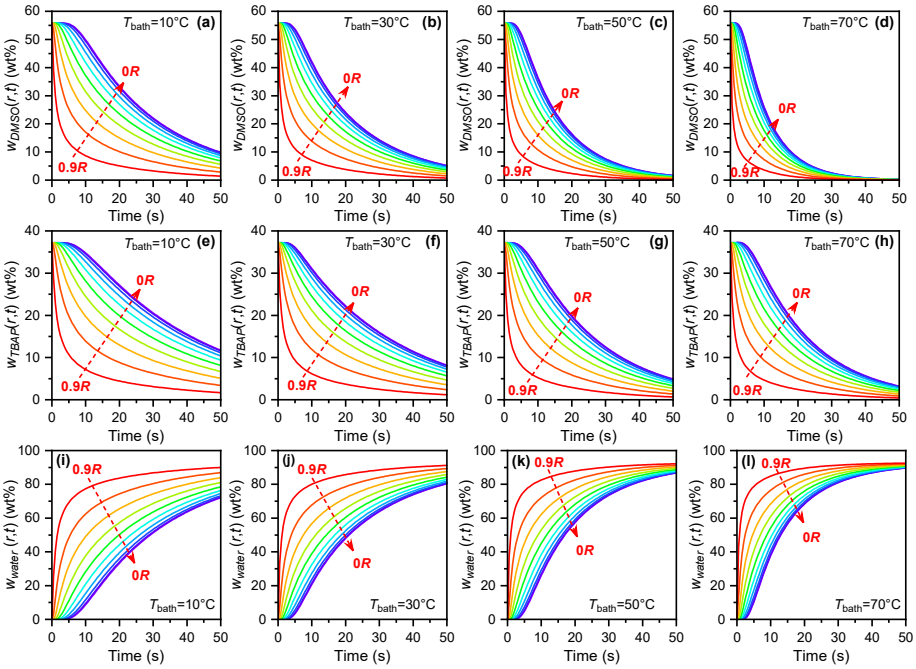


Fig. 8 Evolution of component mass fractions at different radial positions of the filament with coagulation time at different coagulation bath temperatures: (a-d) DMSO, (e-h) TBAP, and (i-l) water. The bath temperatures are 10, 30, 50, and 70 °C, respectively

Fig. 9 shows that the local DMSO and TBAP composition paths at 0.1R and 0.9R start from the same initial composition, separate during coagulation, and approach the same equilibrium composition. At the same local water mass fraction, the near-core region is TBAP-rich, while the near-surface region is DMSO-rich. These descriptions refer to relative compositions at the two positions, rather than net solvent accumulation. This relative composition difference is consistent with the higher D_{app} of DMSO than that of TBAP and reflects different extents of solvent removal. From 10 to 70 °C, the maximum $|\Delta w_{DMSO}|$ increases from approximately 1.8 to 5.6 wt%, while the maximum $|\Delta w_{TBAP}|$ increases from 2.3 to 5.8 wt%. Here, Δw_i denotes the difference between the two positions at the same local water mass fraction. Thus, higher temperatures not only accelerate mass transport but also increase the differences between the radial solvent composition paths. In cellulose/NMMO/water, increasing the temperature from 25 to 65 °C changed the film from a uniform and transparent structure without large voids to an asymmetric cross-section. The high-temperature film contained a dense surface layer, a loose porous middle layer with large voids, and a more uniform inner network (Makarova et al. 2016).

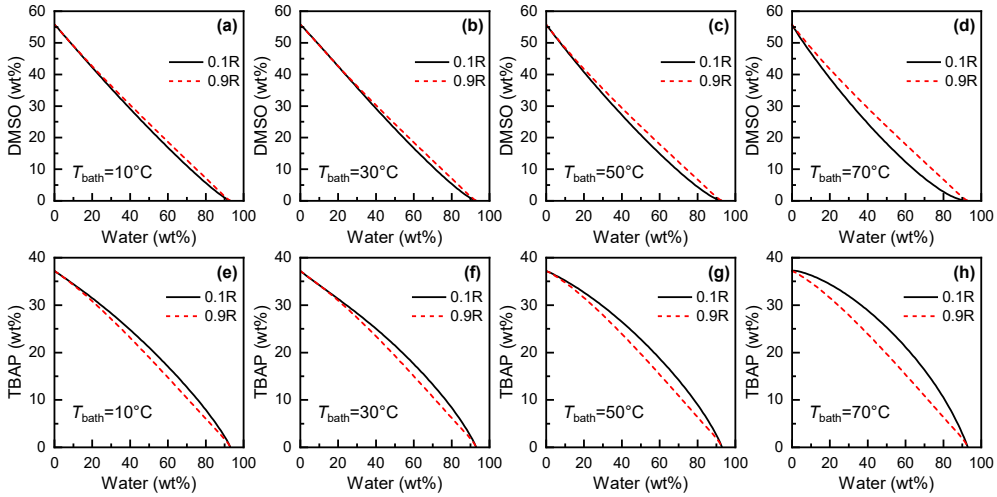


Fig. 9 Evolution of local composition between the near-core (0.1*R*) and near-surface (0.9*R*) positions as a function of local water mass fraction at different coagulation bath temperatures:(a-d) DMSO, (e-h) TBAP

The cloud-point diagrams in **Fig. 10** provide an experimental reference for locating the calculated composition paths relative to the onset of phase separation. DMSO and TBAP are treated as a single component and the cloud-point boundary is determined at a fixed DMSO/TBAP ratio of 1.5. The water mass fraction at the cloud point increased from approximately 7 wt% at 25 °C to 12.5 wt% at 50 °C and 15 wt% at 70 °C. At the intersections with the reference cloud-point boundaries, the calculated DMSO/TBAP ratios at 0.1*R* and 0.9*R* are approximately 1.46 at 10 and 30 °C and 1.35 at 50 °C. At 70 °C, the corresponding ratios are approximately 1.20 near the core and 1.36 near the surface. Thus, the calculated DMSO/TBAP ratios at the intersections with the reference cloud-point boundaries are similar at the two radial positions from 10 to 50 °C but differ at 70 °C. This difference suggests that transport selectivity may affect the local conditions for phase separation through changes in solvent composition. The cloud-point water fractions of about 7-15 wt % indicates that phase separation begins at an early stage of coagulation. Most of the compositions shown in **Fig. 9** lie beyond the cloud-point boundary and within the two-phase region.

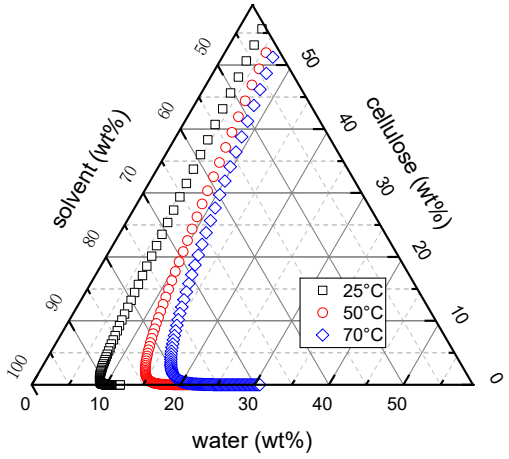


Fig. 10 Pseudo-ternary cloud-point diagrams for cellulose/TBAP/DMSO/water at 25, 50, and 70 °C. Here, DMSO and TBAP are fixed at 1.5 mass ratio

Conclusions

This work identifies radial phase separation as a key link between spinning conditions and skin-core structure formation. This extends coagulation analysis from mass transport to local composition changes during phase separation. The balance between water uptake and solvent loss changed with bath conditions. At low temperatures, water uptake initially exceeded solvent loss, and NMG increased. At 70 °C, NMG was negative from the first measured point. The calculations showed different composition paths in the skin and core at the same water content. From 10 to 70 °C, the maximum differences increased from 1.8 to 5.6 wt% for DMSO and from 2.3 to 5.8 wt% for TBAP. Adding DMSO to the bath generally lowered all three D_{app} values and reduced these differences, although the order of D_{app} remained unchanged. Under the present spinning conditions, the smallest DMSO and TBAP differences occurred at 30 wt% DMSO. Cellulose concentration had only a small effect on D_{app}. Phase separation begins early in coagulation, when the local water content is only 7-15 wt %. Most of the radial composition differences therefore develop inside the two-phase region. Increasing the bath temperature enlarges the skin–core composition difference. At 70 °C the skin and the core enter phase separation from different compositions. Previous studies have generally examined either mass transport or final structure. To the best of our knowledge, the local composition changes linking them have not been quantified for cellulose wet spinning from this system. Their relation to gel formation still requires experimental evidence. Future studies should directly track gel formation during phase separation.

Acknowledgments

This work was supported by the National Natural Science Foundation of China (No. 52273100 and 51873219).

References

Biganska, O., Navard, P. (2005). Kinetics of precipitation of cellulose from cellulose-NMMO-water solutions. *Biomacromolecules* 6: 1948-1953. https://doi.org/10.1021/bm040079q

Boom, R. M., Vandenboomgaard, T., Vandenberg, J. W. A., Smolders, C. A. (1993). Linearized cloudpoint curve correlation for ternary-systems consisting of one polymer, one solvent and one nonsolvent. *Polymer* 34: 2348-2356. https://doi.org/10.1016/0032-3861(93)90819-v

Cai, J., Wang, L. X., Zhang, L. N. (2007). Influence of coagulation temperature on pore size and properties of cellulose membranes prepared from NaOH-urea aqueous solution. *Cellulose* 14: 205-215. https://doi.org/10.1007/s10570-007-9106-3

Cai, J., Zhang, L., Liu, S. L., Liu, Y. T., Xu, X. J., Chen, X. M., Chu, B., Guo, X. L., Xu, J., Cheng, H., Han, C. C., Kuga, S. (2008). Dynamic Self-assembly induced rapid dissolution of cellulose at low temperatures. *Macromolecules* 41: 9345-9351. https://doi.org/10.1021/ma801110g

Crank, J. (1975). *The mathematics of diffusion*. (2nd ed.). Oxford: Oxford University Press.

Fink, H. P., Weigel, P., Purz, H. J., Ganster, J. (2001). Structure formation of regenerated cellulose materials from NMMO-solutions. *Prog Polym Sci* 26: 1473-1524. https://doi.org/10.1016/s0079-6700(01)00025-9

Frickl, H. (1924). A mathematical treatment of the electric conductivity and capacity of disperse systems. I. The electric conductivity of a suspension of homogenous spheroids. *Phys Rev* 24: 575-587. https://doi.org/10.1103/PhysRev.24.575

Guizani, C., Larkiala, S., Moriam, K., Sawada, D., Elsayed, S., Rantasalo, S., Hummel, M., Sixta, H. (2021). Air gap spinning of a cellulose solution in [DBNH][OAc] ionic liquid with a novel vertically arranged spinning bath to simulate a closed loop operation in the Ioncell® process. *J Appl Polym Sci* 138. https://doi.org/10.1002/app.49787

Hauru, L. K. J., Hummel, M., Nieminen, K., Michud, A., Sixta, H. (2016). Cellulose regeneration and spinnability from ionic liquids. *Soft Matter* 12: 1487-1495. https://doi.org/10.1039/c5sm02618k

Hedlund, A., Kohnke, T., Theliander, H. (2017). Diffusion in ionic liquid-cellulose solutions during coagulation in water: Mass transport and coagulation rate measurements. *Macromolecules* 50: 8707-8719. https://doi.org/10.1021/acs.macromol.7b01594

Holda, A. K., Vankelecom, I. F. J. (2015). Understanding and guiding the phase inversion process for synthesis of solvent resistant nanofiltration membranes. *J Appl Polym Sci* 132. https://doi.org/10.1002/app.42130

Idström, A., Gentile, L., Gubitosi, M., Olsson, C., Stenqvist, B., Lund, M., Bergquist, K. E., Olsson, U., Kohnke, T., Bialik, E. (2017). On the dissolution of cellulose in tetrabutylammonium acetate/dimethyl sulfoxide: a frustrated solvent. *Cellulose* 24: 3645-3657. https://doi.org/10.1007/s10570-017-1370-2

Ilyin, S. O., Makarova, V. V., Anokhina, T. S., Ignatenko, V. Y., Brantseva, T. V., Volkov, A. V., Antonov, S. V. (2018). Diffusion and phase separation at the morphology formation of cellulose membranes by regeneration from *N*-methylmorpholine *N*-oxide solutions. *Cellulose* 25: 2515-2530. https://doi.org/10.1007/s10570-018-1756-9

Jiang, G. S., Huang, W. F., Zhu, T. X., Zhang, C. S., Kumi, A. K., Zhang, Y. M., Wang, H. P., Hu, L. J. (2011). Diffusion dynamics of 1-butyl-3-methylimidazolium chloride from cellulose filament during coagulation process. *Cellulose* 18: 921-928. https://doi.org/10.1007/s10570-011-9551-x

Kang, H. L., Liu, R. G., Huang, Y. (2013). Cellulose derivatives and graft copolymers as blocks for functional materials. *Polym Int* 62: 338-344. https://doi.org/10.1002/pi.4455

Kang, H. L., Liu, R. G., Huang, Y. (2015). Graft modification of cellulose: Methods, properties and applications. *Polymer* 70: A1-A16. https://doi.org/10.1016/j.polymer.2015.05.041

Klemm, D., Heublein, B., Fink, H. P., Bohn, A. (2005). Cellulose: Fascinating biopolymer and sustainable raw material. *Angew Chem Int Ed* 44: 3358-3393. https://doi.org/10.1002/anie.200460587

Laity, P. R., Glover, P. M., Hay, J. N. (2002). Composition and phase changes observed by magnetic resonance imaging during non-solvent induced coagulation of cellulose. *Polymer* 43: 5827-5837. https://doi.org/10.1016/S0032-3861(02)00531-1

Liu, C. K., Cuculo, J. A., Smith, B. (1989). Coagulation studies for cellulose in the ammonia/ammonium thiocyanate (NH_3/NH_4SCN) direct solvent system. *J Polym Sci: Polym Phys* 27: 2493-2511. https://doi.org/10.1002/polb.1989.090271208

Liu, C. K., Cuculo, J. A., Smith, B. (1990). Diffusion Competition between solvent and nonsolvent during the coagulation process of cellulose/ammonia/ammonium thiocynate fiber spinning system. *J Polym Sci: Polym Phys* 28: 449-465. https://doi.org/10.1002/polb.1990.090280402

Liu, R. G., Hu, X. C. (2006). Precipitation kinetics of cellulose in the Lyocell spinning process. *Ind Eng Chem Res* 45: 2840-2844. https://doi.org/10.1021/ie050991v

Liu, S. L., Zhang, L. N. (2009). Effects of polymer concentration and coagulation temperature on the properties of regenerated cellulose films prepared from LiOH/urea solution. *Cellulose* 16: 189-198. https://doi.org/10.1007/s10570-008-9268-7

Makarova, V. V., Antonov, S. V., Brantseva, T. V., Kulichikhin, V. G., Anokhina, T. S. (2016). Phase-equilibrium and cellulose-coagulation kinetics for cellulose solutions in *N*-methylmorpholine-*N*-oxide. *Polym Sci Ser A* 58: 732-743. https://doi.org/10.1134/s0965545x1605014x

Marx, M. (1955). Molekulargewichtsbestimmungen an Makromolekularen Stoffen. 39. Viskosimetrische Molekulargewichtsbestimmung von Cellulose in Kupfer-Aethylendiamin. *Makromol Chem* 16: 157-176. https://doi.org/10.1002/macp.1955.020160118

Nishiyama, Y., Asaadi, S., Ahvenainen, P., Sixta, H. (2019). Water-induced crystallization and nano-scale spinodal decomposition of cellulose in NMMO and ionic liquid dope. *Cellulose* 26: 281-289. https://doi.org/10.1007/s10570-018-2148-x

Oh, S. C., Wang, Y. S., Yeo, Y. K. (1996). Modeling and simulation of the coagulation process of poly(acrylonitrile) wet-spinning. *Ind Eng Chem Res* 35: 4796-4800. https://doi.org/10.1021/ie960261a

Quintana, E., Valls, C., Roncero, M. B. (2024). Dissolving-grade pulp: A sustainable source for fiber production. *Wood Sci Technol* 58: 23-85. https://doi.org/10.1007/s00226-023-01519-w

Schenzel, A., Hufendiek, A., Barner-Kowollik, C., Meier, M. A. R. (2014). Catalytic transesterification of cellulose in ionic liquids: sustainable access to cellulose esters. *Green Chem* 16: 3266-3271. https://doi.org/10.1039/c4gc00312h

Shen, H., Sun, T. Y., Zhou, J. P. (2023). Recent progress in regenerated cellulose fibers by wet spinning. *Macromol Mater Eng* 308: 2300089. https://doi.org/10.1002/mame.202300089

Swatloski, R. P., Spear, S. K., Holbrey, J. D., Rogers, R. D. (2002). Dissolution of cellose with ionic liquids. *J Am Chem Soc* 124: 4974-4975. https://doi.org/10.1021/ja025790m

Tu, H., Zhu, M. X., Duan, B., Zhang, L. N. (2021). Recent progress in high-strength and robust regenerated cellulose materials. *Adv Mater* 33: 2000682. https://doi.org/10.1002/adma.202000682

Woodings, C. (2001). *Regenerated cellulose fibres*. Cambridge: Woodhead Publishing.

Wu, J. W., Guo, Z. W., Zhang, T. T., Jiao, Y. F., Kang, H. L., Liu, R. G. (2025). Efficient homogeneous derivatization of cellulose in ditetrabutylammonium hydrogen phosphate/dimethyl sulfoxide. *Cellulose* 32: 7647-7658. https://doi.org/10.1007/s10570-025-06706-5

Wu, J. W., Zhong, Y. L., Kang, H. L., Liu, R. G. (2025). Mechanism of dissolution of cellulose in quaternary ammonium phosphate/dimethyl sulfoxide. *Carbohydr Polym* 352: 123167. https://doi.org/10.1016/j.carbpol.2024.123167

Zhang, D. S., Wang, Y. X., Shi, Z. H. (2019). Influences of diffusion coefficient of 1-allyl-3-methylimidazolium chloride on structure and properties of regenerated cellulose fiber obtained via dry-jet-wet spinning. *J Appl Polym Sci* 136: 47609. https://doi.org/10.1002/app.47609

Zhang, H., Wu, J., Zhang, J., He, J. S. (2005). 1-Allyl-3-methylimidazolium chloride room temperature ionic liquid: A new and powerful nonderivatizing solvent for cellulose. *Macromolecules* 38: 8272-8277. https://doi.org/10.1021/ma0505676

Supplementary Files

This is a list of supplementary files associated with this preprint. Click to download.

- SI0922.docx